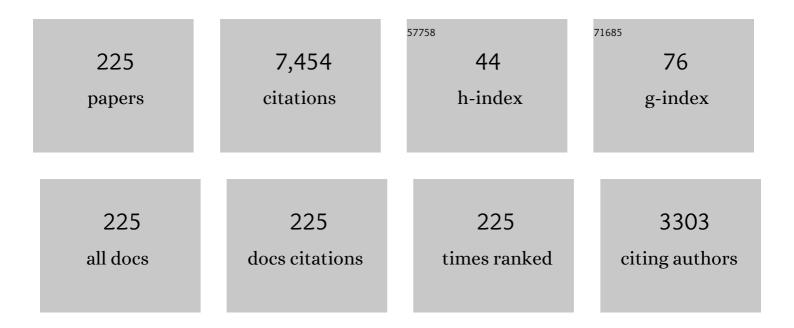
Eiji Akiyama

List of Publications by Year in descending order

Source: https://exaly.com/author-pdf/917105/publications.pdf Version: 2024-02-01



ΕΠΙ ΔΚΙΧΛΜΛ

| # | Article | IF | CITATIONS |
|----|--|-----|-----------|
| 1 | Hydrogen-assisted decohesion and localized plasticity in dual-phase steel. Acta Materialia, 2014, 70, 174-187. | 7.9 | 366 |
| 2 | Effect of hydrogen on the fracture behavior of high strength steel during slow strain rate test. Corrosion Science, 2007, 49, 4081-4097. | 6.6 | 336 |
| 3 | Overview of hydrogen embrittlement in high-Mn steels. International Journal of Hydrogen Energy, 2017, 42, 12706-12723. | 7.1 | 228 |
| 4 | Effect of hydrogen and stress concentration on the notch tensile strength of AISI 4135 steel. Materials Science & Engineering A: Structural Materials: Properties, Microstructure and Processing, 2005, 398, 37-46. | 5.6 | 226 |
| 5 | Hydrogen-assisted failure in a twinning-induced plasticity steel studied under in situ hydrogen charging by electron channeling contrast imaging. Acta Materialia, 2013, 61, 4607-4618. | 7.9 | 218 |
| 6 | Storage and Release of Soluble Hexavalent Chromium from Chromate Conversion Coatings Equilibrium Aspects of Cr[sup VI] Concentration. Journal of the Electrochemical Society, 2000, 147, 2556. | 2.9 | 177 |
| 7 | Hydrogen embrittlement associated with strain localization in a precipitation-hardened Fe–Mn–Al–C light weight austenitic steel. International Journal of Hydrogen Energy, 2014, 39, 4634-4646. | 7.1 | 170 |
| 8 | Hydrogen-induced cracking at grain and twin boundaries in an Fe–Mn–C austenitic steel. Scripta Materialia, 2012, 66, 459-462. | 5.2 | 168 |
| 9 | Review of Hydrogen Embrittlement in Metals: Hydrogen Diffusion, Hydrogen Characterization, Hydrogen Embrittlement Mechanism and Prevention. Acta Metallurgica Sinica (English Letters), 2020, 33, 759-773. | 2.9 | 142 |
| 10 | The role of corrosion-resistant alloying elements in passivity. Corrosion Science, 2007, 49, 42-52. | 6.6 | 137 |
| 11 | Hydrogen embrittlement in a Fe–Mn–C ternary twinning-induced plasticity steel. Corrosion Science, 2012, 54, 1-4. | 6.6 | 134 |
| 12 | Hydrogen degradation of a boron-bearing steel with 1050 and 1300MPa strength levels. Scripta Materialia, 2005, 52, 403-408. | 5.2 | 130 |
| 13 | Determination of the critical hydrogen concentration for delayed fracture of high strength steel by constant load test and numerical calculation. Corrosion Science, 2006, 48, 2189-2202. | 6.6 | 129 |
| 14 | Recent progress in microstructural hydrogen mapping in steels: Quantification, kinetic analysis, and multi-scale characterisation. Materials Science and Technology, 2017, 33, 1481-1496. | 1.6 | 125 |
| 15 | Evaluation of hydrogen entry into high strength steel under atmospheric corrosion. Corrosion Science, 2010, 52, 2758-2765. | 6.6 | 115 |
| 16 | Effect of hydrogen content on the embrittlement in a Fe–Mn–C twinning-induced plasticity steel. Corrosion Science, 2012, 59, 277-281. | 6.6 | 103 |
| 17 | Global CO2 recycling—novel materials and prospect for prevention of global warming and abundant energy supply. Materials Science & Engineering A: Structural Materials: Properties, Microstructure and Processing, 1999, 267, 200-206. | 5.6 | 99 |
| 18 | Crosshead speed dependence of the notch tensile strength of a high strength steel in the presence of hydrogen. Scripta Materialia, 2005, 53, 713-718. | 5.2 | 99 |

| # | Article | IF | CITATIONS |
|----|--|-----|-----------|
| 19 | Anodically deposited manganese oxide and manganese–tungsten oxide electrodes for oxygen evolution from seawater. Electrochimica Acta, 1998, 43, 3303-3312. | 5.2 | 96 |
| 20 | Hydrogen-assisted quasi-cleavage fracture in a single crystalline type 316 austenitic stainless steel. Corrosion Science, 2013, 75, 345-353. | 6.6 | 85 |
| 21 | Hydrogen entry into Fe and high strength steels under simulated atmospheric corrosion. Electrochimica Acta, 2011, 56, 1799-1805. | 5.2 | 77 |
| 22 | Title is missing!. Journal of Applied Electrochemistry, 1999, 29, 769-775. | 2.9 | 74 |
| 23 | Evaluation of Delayed Fracture Characteristics of High Strength Steel based on CSRT Method. Tetsu-To-Hagane/Journal of the Iron and Steel Institute of Japan, 2008, 94, 215-221. | 0.4 | 70 |
| 24 | Evaluation of susceptibility of high strength steels to delayed fracture by using cyclic corrosion test and slow strain rate test. Corrosion Science, 2010, 52, 1660-1667. | 6.6 | 69 |
| 25 | Experimental evidence for the critical size of heterogeneity areas for pitting corrosion of Cr-Zr alloys in 6 M HCl. Corrosion Science, 1998, 40, 1-17. | 6.6 | 68 |
| 26 | The effect of air exposure on the corrosion behavior of amorphous Fe-8Cr-Mo-13P-7C alloys in 1 M HCl. Corrosion Science, 1995, 37, 1289-1301. | 6.6 | 67 |
| 27 | Characterization of sputter-deposited Ni-Mo and Ni-W alloy electrocatalysts for hydrogen evolution in alkaline solution. Materials Science & Engineering A: Structural Materials: Properties, Microstructure and Processing, 1997, 226-228, 905-909. | 5.6 | 67 |
| 28 | Oxygen evolution on manganese–molybdenum oxide anodes in seawater electrolysis. Materials Science & Engineering A: Structural Materials: Properties, Microstructure and Processing, 1999, 267, 254-259. | 5.6 | 65 |
| 29 | Spatially and Kinetically Resolved Mapping of Hydrogen in a Twinning-Induced Plasticity Steel by Use of Scanning Kelvin Probe Force Microscopy. Journal of the Electrochemical Society, 2015, 162, C638-C647. | 2.9 | 64 |
| 30 | Compositional dependence of the CO2 methanation activity of Ni/ZrO2 catalysts prepared from amorphous NiZr alloy precursors. Applied Catalysis A: General, 1997, 163, 187-197. | 4.3 | 61 |
| 31 | Hydrogen Embrittlement of a 1500-MPa Tensile Strength Level Steel with an Ultrafine Elongated Grain Structure. Metallurgical and Materials Transactions A: Physical Metallurgy and Materials Science, 2012, 43, 1670-1687. | 2.2 | 61 |
| 32 | Recent progress in corrosion-resistant metastable alloys. Materials Science & Engineering A: Structural Materials: Properties, Microstructure and Processing, 1995, 198, 1-10. | 5.6 | 57 |
| 33 | CO2 methanation catalysts prepared from amorphous Ni–Zr–Sm and Ni–Zr–misch metal alloy precursors. Materials Science & Engineering A: Structural Materials: Properties, Microstructure and Processing, 1999, 267, 220-226. | 5.6 | 57 |
| 34 | The corrosion behavior of sputter-deposited amorphous titanium-chromium alloys in 1 M and 6 M HCl solutions. Corrosion Science, 1993, 34, 975-987. | 6.6 | 55 |
| 35 | Materials for global carbon dioxide recycling. Corrosion Science, 2002, 44, 371-386. | 6.6 | 55 |
| 36 | Effects of severe plastic deformation on the corrosion behavior of aluminum alloys. Journal of Solid State Electrochemistry, 2009, 13, 277-282. | 2.5 | 55 |

| # | Article | IF | CITATIONS |
|----|---|-----|-----------|
| 37 | Advanced materials for global carbon dioxide recycling. Materials Science & Engineering A: Structural Materials: Properties, Microstructure and Processing, 2001, 304-306, 88-96. | 5.6 | 54 |
| 38 | The corrosion behavior of sputter-deposited amorphous chromium-zirconium alloys in 6 M HCl solution. Corrosion Science, 1993, 34, 1817-1827. | 6.6 | 53 |
| 39 | The role of chromium and molybdenum in passivation of amorphous Fe-Cr-Mo-P-C alloys in deaerated 1 M HCl. Corrosion Science, 1996, 38, 2137-2151. | 6.6 | 53 |
| 40 | The passivation behavior of sputter-deposited W-Ta alloys in 12 M HCl. Corrosion Science, 1998, 40, 757-779. | 6.6 | 53 |
| 41 | The corrosion behavior of sputter-deposited Mo-Ti alloys in concentrated hydrochloric acid. Corrosion Science, 1996, 38, 1649-1667. | 6.6 | 51 |
| 42 | Hydrogen embrittlement property of a 1700-MPa-class ultrahigh-strength tempered martensitic steel. Science and Technology of Advanced Materials, 2010, 11, 025005. | 6.1 | 51 |
| 43 | Hydrogen-induced delayed fracture of a Fe–22Mn–0.6C steel pre-strained at different strain rates. Scripta Materialia, 2012, 66, 947-950. | 5.2 | 50 |
| 44 | Effect of α-Al/Al3Ni microstructure on the corrosion behaviour of Al–5.4wt% Ni alloy fabricated by equal-channel angular pressing. Corrosion Science, 2007, 49, 2962-2972. | 6.6 | 47 |
| 45 | The corrosion behavior of sputter-deposited amorphous Crî—,Nb and Crî—,Ta alloys in 12 M HCl solution. Corrosion Science, 1993, 34, 1947-1955. | 6.6 | 46 |
| 46 | Storage and Release of Soluble Hexavalent Chromium from Chromate Conversion Coatings on Al Alloys: Kinetics of Release. Journal of the Electrochemical Society, 2003, 150, B83. | 2.9 | 46 |
| 47 | Evaluation of Delayed Fracture Property of High Strength Bolt Steels. ISIJ International, 2012, 52, 307-315. | 1.4 | 45 |
| 48 | The corrosion behavior of sputter-deposited amorphous Mo-Zr alloys in 12 M HCl. Corrosion Science, 1995, 37, 307-320. | 6.6 | 43 |
| 49 | Studies of Evaluation of Hydrogen Embrittlement Property of High-Strength Steels with Consideration of the Effect of Atmospheric Corrosion. Metallurgical and Materials Transactions A: Physical Metallurgy and Materials Science, 2013, 44, 1290-1300. | 2.2 | 43 |
| 50 | Tensile mechanical properties and fracture behaviors of nickel-based superalloy 718 in the presence of hydrogen. International Journal of Hydrogen Energy, 2018, 43, 20118-20132. | 7.1 | 42 |
| 51 | An XPS study of passive films on corrosion-resistant Crî—,Zr alloys prepared by sputter deposition. Corrosion Science, 1997, 39, 1365-1380. | 6.6 | 41 |
| 52 | Corrosion-resistant amorphous surface alloys. Corrosion Science, 1993, 35, 363-370. | 6.6 | 40 |
| 53 | Fracture criterion for hydrogen embrittlement of high strength steel. Materials Science and Technology, 2006, 22, 167-172. | 1.6 | 40 |
| 54 | The corrosion behavior of sputter-deposited amorphous Wî—,Ti alloys in 6 M HCl solution. Corrosion Science, 1995, 37, 2071-2086. | 6.6 | 39 |

| # | Article | IF | CITATIONS |
|----|---|-----|-----------|
| 55 | The corrosion behavior of sputter-deposited Moî—,Ta alloys in 12 M HCl solution. Corrosion Science, 1996, 38, 397-411. | 6.6 | 39 |
| 56 | An XPS study of the corrosion behavior of sputter-deposited amorphous Cr-Nb and Cr-Ta alloys in 12 M HCl solution. Corrosion Science, 1994, 36, 511-523. | 6.6 | 38 |
| 57 | The effect of heat treatment on the corrosion behavior of sputter-deposited aluminum–chromium alloys. Corrosion Science, 1998, 41, 477-499. | 6.6 | 38 |
| 58 | Microstructural and crystallographic study of hydrogen-assisted cracking in high strength PSB1080 steel. International Journal of Hydrogen Energy, 2018, 43, 17898-17911. | 7.1 | 38 |
| 59 | Electrochemical and xps studies of the corrosion behavior of sputter-deposited amorphous W-Zr alloys in 6 and 12 M HCl solutions. Corrosion Science, 1997, 39, 355-375. | 6.6 | 37 |
| 60 | Room-temperature blue brittleness of Fe-Mn-C austenitic steels. Scripta Materialia, 2017, 141, 20-23. | 5.2 | 37 |
| 61 | The Influence of Dichromate Ions on Aluminum Dissolution Kinetics in Artificial Crevice Electrode Cells. Journal of the Electrochemical Society, 1999, 146, 4095-4100. | 2.9 | 35 |
| 62 | Hydrogen Embrittlement in Al-added Twinning-induced Plasticity Steels Evaluated by Tensile Tests during Hydrogen Charging. ISIJ International, 2012, 52, 2283-2287. | 1.4 | 35 |
| 63 | The corrosion behavior of sputter-deposited Mo-Nb alloys in 12 M HCl solution. Corrosion Science, 1996, 38, 1731-1750. | 6.6 | 34 |
| 64 | Effects of Additional Elements on Electrocatalytic Properties of Thermally Decomposed Manganese Oxide Electrodes for Oxygen Evolution from Seawater. Materials Transactions, JIM, 1997, 38, 899-905. | 0.9 | 34 |
| 65 | Evaluation of delayed fracture property of outdoor-exposed high strength AISI 4135 steels. Corrosion Science, 2010, 52, 3198-3204. | 6.6 | 34 |
| 66 | Martensitic transformation-induced hydrogen desorption characterized by utilizing cryogenic thermal desorption spectroscopy during cooling. Scripta Materialia, 2016, 122, 50-53. | 5.2 | 34 |
| 67 | The corrosion behavior of sputter-deposited Cr-Mo alloys in 12 M HCl solution. Corrosion Science, 1995, 37, 1843-1860. | 6.6 | 33 |
| 68 | Electrochemical and XPS studies of the corrosion behavior of sputter-deposited W-Nb alloys in concentrated hydrochloric acid solutions. Corrosion Science, 1998, 40, 19-42. | 6.6 | 32 |
| 69 | Corrosion behaviour of sputter-deposited Mg–Zr alloys in a borate buffer solution. Corrosion Science, 2011, 53, 2988-2993. | 6.6 | 32 |
| 70 | Comparison of Constant Load, SSRT and CSRT Methods for Hydrogen Embrittlement Evaluation Using Round Bar Specimens of High Strength Steels. ISIJ International, 2016, 56, 1268-1275. | 1.4 | 32 |
| 71 | Effect of Strain Rate on the Hydrogen Embrittlement Property of Ultra High-strength Low Alloy TRIP-aided Steel. ISIJ International, 2018, 58, 751-759. | 1.4 | 32 |
| 72 | Surface activation of manganese oxide electrode for oxygen evolution from seawater. Journal of Applied Electrochemistry, 1997, 27, 1362-1368. | 2.9 | 31 |

| # | Article | IF | CITATIONS |
|----|--|------|-----------|
| 73 | Electrochemical and XPS studies on the passivation behavior of sputter-deposited W-Cr Alloys in 12 M HCl solution. Corrosion Science, 1998, 40, 155-175. | 6.6 | 31 |
| 74 | The corrosion behavior of sputter-deposited amorphous Cr-Ni-Mo alloys in 12 M HCl. Corrosion Science, 1994, 36, 1395-1410. | 6.6 | 30 |
| 75 | Constant-load delayed fracture test of atmospherically corroded high strength steels. Applied Surface Science, 2011, 257, 8275-8281. | 6.1 | 30 |
| 76 | Effect of heat treatment on hydrogen-assisted fracture behavior of PH13-8Mo steel. Corrosion Science, 2017, 128, 198-212. | 6.6 | 30 |
| 77 | Effects of Mn Content and Grain Size on Hydrogen Embrittlement Susceptibility of Face-Centered Cubic High-Entropy Alloys. Metallurgical and Materials Transactions A: Physical Metallurgy and Materials Science, 2020, 51, 5612-5616. | 2.2 | 30 |
| 78 | The corrosion behavior of sputter-deposited amorphous Alî—,Crî—,Mo alloys in 1 M HCl. Corrosion Science, 1996, 38, 279-292. | 6.6 | 29 |
| 79 | The corrosion behaviour of sputter-deposited amorphous Mn-Ti alloys in 0.5 M NaCl solutions. Corrosion Science, 1997, 39, 305-320. | 6.6 | 29 |
| 80 | Electrochemical hydrogen permeation tests under galvanostatic hydrogen charging conditions conventionally used for hydrogen embrittlement study. Corrosion Reviews, 2016, 34, 103-112. | 2.0 | 29 |
| 81 | The influences of Mo addition and air exposure on the corrosion behavior of amorphous Feî—,8Crî—,13Pî—,7C alloy in de-aerated 1 M HCl. Corrosion Science, 1996, 38, 349-365. | 6.6 | 27 |
| 82 | Spontaneously passivated films on sputter-deposited Cr-Ti alloys in 6 M HCl solution. Corrosion Science, 1997, 39, 935-948. | 6.6 | 27 |
| 83 | The corrosion behavior of amorphous and crystalline Ni-10Ta-20P alloys in 12 M HCl. Corrosion Science, 1996, 38, 1269-1279. | 6.6 | 26 |
| 84 | Hydrogen embrittlement of high strength steam turbine last stage blade steels: Comparison between PH17-4 steel and PH13-8Mo steel. Materials Science & Engineering A: Structural Materials: Properties, Microstructure and Processing, 2019, 742, 353-363. | 5.6 | 26 |
| 85 | Hydrogen-assisted damage in austenite/martensite dual-phase steel. Philosophical Magazine Letters, 2016, 96, 9-18. | 1.2 | 25 |
| 86 | Effects of Static and Dynamic Strain Aging on Hydrogen Embrittlement in TWIP Steels Containing Al. ISIJ International, 2013, 53, 1268-1274. | 1.4 | 24 |
| 87 | Hydrogen embrittlement behavior of Inconel 718 alloy at room temperature. Journal of Materials Science and Technology, 2019, 35, 499-502. | 10.7 | 24 |
| 88 | Effect of hydrogen charging time on hydrogen blister and hydrogen-induced cracking of pure iron. Corrosion Science, 2021, 181, 109200. | 6.6 | 24 |
| 89 | The degradation of the corrosion resistance of sputter-deposited chromium–titanium alloys by nanoscale heterogeneity. Corrosion Science, 1999, 41, 1871-1890. | 6.6 | 23 |
| 90 | Comparison of Constant Load, SSRT and CSRT Methods for Hydrogen Embrittlement Evaluation Using Round Bar Specimens of High Strength Steels. Tetsu-To-Hagane/Journal of the Iron and Steel Institute of Japan, 2014, 100, 1298-1305. | 0.4 | 23 |

| # | Article | IF | CITATIONS |
|-----|--|-----|-----------|
| 91 | Transformation-assisted hydrogen desorption during deformation in steels: Examples of α′- and ε-Martensite. International Journal of Hydrogen Energy, 2019, 44, 30472-30477. | 7.1 | 23 |
| 92 | The corrosion behaviour of sputter-deposited amorphous Niî—,Ti alloys in 1 M HCl. Materials Science & Engineering A: Structural Materials: Properties, Microstructure and Processing, 1994, 181-182, 1128-1132. | 5.6 | 21 |
| 93 | The effects of alloying elements on the passivity of sputter-deposited amorphous Al-Cr-Mo alloys in 1M HCl. Corrosion Science, 1996, 38, 1281-1294. | 6.6 | 21 |
| 94 | A study of the structure of a passive film using angle-resolved X-ray photo-electron spectroscopy. Corrosion Science, 1996, 38, 1127-1140. | 6.6 | 21 |
| 95 | The corrosion behavior of sputter-deposited amorphous Fe–Cr–Ni–Ta alloys in 12 M HCl. Corrosion Science, 1999, 41, 1849-1869. | 6.6 | 21 |
| 96 | Hydrogen Visualization in Steels Using Ag Decoration Method. Materials Transactions, 2015, 56, 793-797. | 1.2 | 21 |
| 97 | Effects of Alloying Elements Addition on Delayed Fracture Properties of Ultra High-Strength TRIP-Aided Martensitic Steels. Metals, 2020, 10, 6. | 2.3 | 21 |
| 98 | Effects of residual stress and plastic strain on hydrogen embrittlement of a stretch-formed TRIP-aided martensitic steel sheet. Corrosion Science, 2020, 177, 108957. | 6.6 | 21 |
| 99 | Warm tempforming effect on the hydrogen embrittlement of 1.8-GPa-class ultra-high-strength low-alloy steel. Materials Science & Engineering A: Structural Materials: Properties, Microstructure and Processing, 2017, 703, 503-512. | 5.6 | 20 |
| 100 | Interfacial hydrogen localization in austenite/martensite dualâ€phase steel visualized through optimized silver decoration and scanning Kelvin probe force microscopy. Materials and Corrosion - Werkstoffe Und Korrosion, 2017, 68, 306-310. | 1.5 | 20 |
| 101 | Strain rate and hydrogen effects on crack growth from a notch in a Fe-high-Mn steel containing 1.1Âwt% solute carbon. International Journal of Hydrogen Energy, 2020, 45, 1125-1139. | 7.1 | 19 |
| 102 | Distribution of Hydrogen Occluded in Bolts Tightened beyond the Yield Strength and Exposed at a Seashore Site. Tetsu-To-Hagane/Journal of the Iron and Steel Institute of Japan, 2002, 88, 849-856. | 0.4 | 19 |
| 103 | Total Synthesis and Absolute Configuration of (-)-Sedacryptine. Synlett, 1996, 1996, 100-102. | 1.8 | 18 |
| 104 | The roles of tantalum and phosphorus in the corrosion behavior of Ni-Ta-P alloys in 12 M HCl. Corrosion Science, 1997, 39, 321-332. | 6.6 | 18 |
| 105 | An XPS study of passive films on sputter-deposited Cr-Nb alloys in 12 M HCl solution. Corrosion Science, 1998, 40, 821-838. | 6.6 | 18 |
| 106 | High-concentration carbon assists plasticity-driven hydrogen embrittlement in a Fe-high Mn steel with a relatively high stacking fault energy. Materials Science & Engineering A: Structural Materials: Properties, Microstructure and Processing, 2018, 717, 78-84. | 5.6 | 18 |
| 107 | Role of mill scale on corrosion behavior of steel rebars in mortar. Corrosion Science, 2020, 177, 108995. | 6.6 | 18 |
| 108 | Hydrogen embrittlement resistance of pre-strained ultra-high-strength low alloy TRIP-aided steel. International Journal of Fracture, 2020, 224, 253-260. | 2.2 | 18 |

| # | Article | IF | CITATIONS |
|-----|---|-----|-----------|
| 109 | Hydrogen Entry Behavior into Iron and Steel under Atmospheric Corrosion. ISIJ International, 2013, 53, 1062-1069. | 1.4 | 18 |
| 110 | The corrosion behaviour of sputter-deposited amorphous Mn-Ta alloys in 0.5 M NaCl solution. Corrosion Science, 1997, 39, 1965-1979. | 6.6 | 17 |
| 111 | XPS and electrochemical studies on the corrosion behaviour of sputter-deposited amorphous Mn-Nb alloys in a neutral chloride solution. Corrosion Science, 1998, 40, 1513-1531. | 6.6 | 17 |
| 112 | Effects of Oxygen Pressure and Chloride Ion Concentration on Corrosion of Iron in Mortar Exposed to Pressurized Humid Oxygen Gas. Journal of the Electrochemical Society, 2018, 165, C582-C589. | 2.9 | 17 |
| 113 | Pre-strain effects on critical stress and hydrogen content for hydrogen-induced quasi-cleavage fracture in a TRIP-aided bainitic ferrite steel: Martensitic transformation, matrix damage, and strain aging. International Journal of Hydrogen Energy, 2020, 45, 27920-27928. | 7.1 | 17 |
| 114 | Effect of austempering treatment on the microstructure and mechanical properties of 0.4C–1.5Si-1.5Mn TRIP-aided bainitic ferrite steel. Materials Science & Engineering A: Structural Materials: Properties, Microstructure and Processing, 2021, 819, 141479. | 5.6 | 17 |
| 115 | Electrochemical and XPS studies of the effects of alloying elements on the corrosion behavior of amorphous Feî—,Crî—,Metalloid alloys in 9 M H2SO4. Corrosion Science, 1993, 34, 1829-1839. | 6.6 | 16 |
| 116 | The corrosion behavior of amorphous Fe-8Cr-13P-7C and Fe-8Cr-20P alloys in concentrated sulfuric acid. Corrosion Science, 1994, 36, 1537-1550. | 6.6 | 16 |
| 117 | The effect of phosphorus addition on the corrosion behavior of amorphous Ni-30Ta-P alloys in 12 M HCl. Corrosion Science, 1995, 37, 321-330. | 6.6 | 16 |
| 118 | Global CO2 Recycling. Zairyo To Kankyo/ Corrosion Engineering, 1996, 45, 614-620. | 0.2 | 16 |
| 119 | Corrosion-resistant amorphous aluminum alloys and structure of passive films. Materials Science & Engineering A: Structural Materials: Properties, Microstructure and Processing, 1997, 226-228, 920-924. | 5.6 | 16 |
| 120 | Effects of nanocrystalline heterogeneity on the corrosion behavior of sputter-deposited chromium–niobium alloys. Corrosion Science, 2000, 42, 361-382. | 6.6 | 16 |
| 121 | Interstitial Carbon Enhanced Corrosion Resistance of Fe-33Mn-xC Austenitic Steels: Inhibition of Anodic Dissolution. Journal of the Electrochemical Society, 2018, 165, C19-C26. | 2.9 | 16 |
| 122 | Hydrogen embrittlement and associated surface crack growth in fine-grained equiatomic CoCrFeMnNi high-entropy alloys with different annealing temperatures evaluated by tensile testing under in situ hydrogen charging. International Journal of Hydrogen Energy, 2021, 46, 33028-33038. | 7.1 | 16 |
| 123 | The effect of phosphorus addition on the corrosion behavior of amorphous Fe-8Cr-P alloys in 9M H2SO4. Corrosion Science, 1995, 37, 709-722. | 6.6 | 15 |
| 124 | Mn–W Oxide Anodes Prepared by Thermal Decomposition for Oxygen Evolution in Seawater Electrolysis. Materials Transactions, JIM, 1998, 39, 308-313. | 0.9 | 15 |
| 125 | The effect of magnesium on the corrosion behavior of sputter-deposited amorphous Alî—,Mgî—,Ti ternary alloys in a neutral chloride solution. Corrosion Science, 1993, 34, 27-40. | 6.6 | 14 |
| 126 | Change in the surface composition of amorphous Feî—,Crî—,Moî—,Pî—,C alloys during air exposure. Corrosion Science, 1995, 37, 331-341. | 6.6 | 14 |

| # | Article | IF | CITATIONS |
|-----|--|-----|-----------|
| 127 | High Temperature Sulfidation and Oxidation Behavior of Sputter-Deposited Al-refractory Metal Alloys. Materials Transactions, JIM, 1996, 37, 379-382. | 0.9 | 14 |
| 128 | Electrochemical and XPS studies of the passivation behavior of sputter-deposited Cr–Ta alloys in 12 M HCl. Corrosion Science, 1998, 40, 1587-1604. | 6.6 | 14 |
| 129 | Characterization of CO2 methanation catalysts prepared from amorphous Ni-Zr and NI-Zr-rare earth element alloys. Studies in Surface Science and Catalysis, 1998, 114, 451-454. | 1.5 | 14 |
| 130 | Hydrogen mapping across a crevice: Effect of applied potential. Scripta Materialia, 2005, 53, 1219-1223. | 5.2 | 14 |
| 131 | Fretting fatigue behaviour of Ni-free high-nitrogen stainless steel in a simulated body fluid. Science and Technology of Advanced Materials, 2013, 14, 025002. | 6.1 | 14 |
| 132 | Quantitative Evaluation of Hydrogen Effects on Evolutions of Deformation-Induced ε-Martensite and Damage in a High-Mn Steel. Metallurgical and Materials Transactions A: Physical Metallurgy and Materials Science, 2020, 51, 6184-6194. | 2.2 | 14 |
| 133 | An angle-resolved xps study of the in-depth structure of passivated amorphous aluminum alloys. Corrosion Science, 1997, 39, 1351-1364. | 6.6 | 13 |
| 134 | Strain rate sensitivity of hydrogen-assisted Îμ-martensitic transformation and associated hydrogen embrittlement in high-Mn steel. International Journal of Hydrogen Energy, 2021, 46, 27221-27233. | 7.1 | 13 |
| 135 | Hydrogen Mapping Across Crevices. Electrochemical and Solid-State Letters, 2005, 8, B30. | 2.2 | 12 |
| 136 | Detection of hydrogen effusion before, during, and after martensitic transformation: Example of multiphase transformation-induced plasticity steel. International Journal of Hydrogen Energy, 2019, 44, 26028-26035. | 7.1 | 12 |
| 137 | Lowering Strain Rate Simultaneously Enhances Carbon- and Hydrogen-Induced Mechanical Degradation in an Fe-33Mn-1.1C Steel. Metallurgical and Materials Transactions A: Physical Metallurgy and Materials Science, 2019, 50, 1137-1141. | 2.2 | 12 |
| 138 | Application of an iridium complex for detecting hydrogen permeation through pure iron. International Journal of Hydrogen Energy, 2020, 45, 25580-25586. | 7.1 | 12 |
| 139 | Activation energy of hydrogen desorption from high-performance titanium oxide carrier-selective contacts with silicon oxide interlayers. Current Applied Physics, 2021, 21, 36-42. | 2.4 | 12 |
| 140 | The effect of phosphorus on the passivation behavior of Ni-10Ta-P alloys in 12 M HCl. Corrosion Science, 1995, 37, 1313-1324. | 6.6 | 11 |
| 141 | The effect of molybdenum on the stability of passive films formed on amorphous Fe-Cr-Mo-P-C alloys by potentiostatic polarization in deaerated 1 M HCl. Corrosion Science, 1997, 39, 589-603. | 6.6 | 11 |
| 142 | The effect of alloying elements on the corrosion behaviour of sputter-deposited amorphous Mn–Ta–Cr alloys in 1 M H2SO4. Corrosion Science, 1998, 40, 1491-1512. | 6.6 | 11 |
| 143 | Electrochemical and XPS studies of the corrosion behavior of sputter-deposited amorphous Fe–Cr–Ni–Nb alloys in 6 M HCl. Corrosion Science, 1999, 41, 1095-1118. | 6.6 | 11 |
| 144 | Discrete electrochemical transients of aluminium alloys generated by slurry jet impingement. Journal Physics D: Applied Physics, 2006, 39, 3157-3164. | 2.8 | 11 |

| # | ARTICLE | IF | CITATIONS |
|-----|--|------|-----------|
| 145 | Nitrogen monoxide decomposition catalysts prepared from amorphous Ni-valve metal-Pd alloys. Materials Science & Engineering A: Structural Materials: Properties, Microstructure and Processing, 1994, 181-182, 1123-1127. | 5.6 | 10 |
| 146 | Decomposition of nitrogen monoxide over NiTa2O6-supported palladium catalysts prepared from amorphous alloy precursors. Applied Catalysis B: Environmental, 1996, 9, 93-106. | 20.2 | 10 |
| 147 | Electrochemical Hydrogen Permeation Tests under Conventional Potentiostatic Hydrogen Charging Conditions Conventionally Used for Hydrogen Embrittlement Study. ECS Transactions, 2017, 75, 23-31. | 0.5 | 10 |
| 148 | An Evaluation Method for Hydrogen Embrittlement of High Strength Steel Sheets Using U-bend Specimens. Tetsu-To-Hagane/Journal of the Iron and Steel Institute of Japan, 2019, 105, 927-934. | 0.4 | 10 |
| 149 | Hyperbaric-Oxygen Accelerated Corrosion Test for Iron in Cement Paste and Mortar. Materials Transactions, 2018, 59, 927-934. | 1.2 | 10 |
| 150 | Preface to the Special Issue on "Common Bases for Hydrogen Embrittlement Studies― ISIJ International, 2012, 52, 167. | 1.4 | 10 |
| 151 | The influence of concentration of hydrochloric acid solutions on the passivation behavior of sputter-deposited tungsten rich W–Nb alloys. Corrosion Science, 1998, 40, 1897-1914. | 6.6 | 9 |
| 152 | Factors Affecting Static Strain Aging under Stress at Room Temperature in a Fe–Mn–C Twinning-induced Plasticity Steel. ISIJ International, 2013, 53, 1089-1096. | 1.4 | 9 |
| 153 | Electrochemical Hydrogen Permeation Test under Controlled Temperature and Humidity after Outdoor Exposure at Beijing, Chongqing and Okinawa. ISIJ International, 2016, 56, 436-443. | 1.4 | 9 |
| 154 | Depassivation and Repassivation of Titanium under Particle Impingements. ECS Transactions, 2006, 1, 437-446. | 0.5 | 8 |
| 155 | The Use of Renewable Energy in the Form of Methane Via Electrolytic Hydrogen Generation / Zastosowanie Odnawialnej Energii W Formie Metanu Na Drodze Elektrolitycznej Produkcji Wodoru. Archives of Metallurgy and Materials, 2013, 58, 231-239. | 0.6 | 8 |
| 156 | Hydrogen Visualization in Steels Using Ag Decoration Method. Nippon Kinzoku Gakkaishi/Journal of the Japan Institute of Metals, 2013, 77, 622-626. | 0.4 | 8 |
| 157 | Hydrogen embrittlement properties of nitrogen added ultra-high-strength TRIP-aided martensitic steels evaluated by using conventional strain rate technique. Procedia Manufacturing, 2018, 15, 1581-1587. | 1.9 | 8 |
| 158 | Multiple damage mechanisms facilitated by planar dislocation glide in a commercial-grade precipitation-strengthened Fe–Ni–Cr-based steel. Materials Science & Engineering A: Structural Materials: Properties, Microstructure and Processing, 2020, 782, 139250. | 5.6 | 8 |
| 159 | Hydrogen Entry in Crevice Region: Evaluation by Hydrogen Permeation Technique. ISIJ International, 2006, 46, 1081-1085. | 1.4 | 8 |
| 160 | Preparation of Protective Multilayer SiO2 and Al2O3 Coatings on Austenitic Stainless Steel by Sol-Gel Method. Zairyo To Kankyo/ Corrosion Engineering, 1994, 43, 654-659. | 0.2 | 7 |
| 161 | Amorphous Fe-valve metal-Pt group metal alloy catalysts for methanation of CO2. Materials Science & Engineering A: Structural Materials: Properties, Microstructure and Processing, 1994, 181-182, 1133-1136. | 5.6 | 7 |
| 162 | Hydrogen Thermal Desorption Analysis for the Studies of Hydrogen Embrittlement of High Strength Steels. Journal of the Vacuum Society of Japan, 2014, 57, 207-213. | 0.3 | 7 |

| # | Article | IF | CITATIONS |
|-----|--|-----|-----------|
| 163 | Hydrogen-assisted damage evolution in nitrogen-doped duplex stainless steel. International Journal of Hydrogen Energy, 2021, 46, 2716-2728. | 7.1 | 7 |
| 164 | Availability of Opal Photonic Crystal Films for Visualizing Heterogeneous Strain Evolution in Steels: Example of Lüders Deformation. ISIJ International, 2020, 60, 2604-2608. | 1.4 | 7 |
| 165 | Amorphous alloy catalysts for decomposition of CCl2F2 by hydrolysis. Materials Science & Engineering A: Structural Materials: Properties, Microstructure and Processing, 1994, 181-182, 1091-1094. | 5.6 | 6 |
| 166 | The influence of pre-immersion on the potentiostatic polarization behavior of amorphous Fe-Cr-Mo-P-C alloys in de-aerated 1 M HCl. Corrosion Science, 1996, 38, 1495-1511. | 6.6 | 6 |
| 167 | The effect of phosphorus addition on the corrosion behavior of ARC-MELTED Niî—,10Taî—,P alloys in 12 M HCl. Corrosion Science, 1996, 38, 469-485. | 6.6 | 6 |
| 168 | The sulfidation and oxidation behavior of sputter-deposited Cr-refractory metal alloys at high temperatures. Materials Science & Engineering A: Structural Materials: Properties, Microstructure and Processing, 1997, 226-228, 910-914. | 5.6 | 6 |
| 169 | Passivity and its breakdown on sputter-deposited amorphous Mn-Zr alloys in neutral chloride solutions. Corrosion Science, 1998, 40, 235-250. | 6.6 | 6 |
| 170 | Corrosion-resistant Mnî—,Zrî—,Cr alloys in chloride-containing media. Materials Science & Engineering A: Structural Materials: Properties, Microstructure and Processing, 1999, 267, 285-293. | 5.6 | 6 |
| 171 | Effect of Hydrogen on the Fracture Behavior of High-Strength Cr-Mo Steel. Materials Science Forum, 2006, 512, 55-60. | 0.3 | 6 |
| 172 | Effects of Hydrogen on Tensile Properties at Slow Strain Rate of Ultra High-Strength TRIP-aided Bainitic Ferrite Steels. Procedia Engineering, 2017, 207, 1868-1873. | 1.2 | 6 |
| 173 | Hydrogen Enhances Shape Memory Effect of a Ferrous Face-Centered Cubic Alloy. Metallurgical and Materials Transactions A: Physical Metallurgy and Materials Science, 2020, 51, 4439-4441. | 2.2 | 6 |
| 174 | Decomposition of Nitrogen Monoxide over Amorphous Co–65Zr Alloys Containing Platinum Group Elements. Materials Transactions, JIM, 1993, 34, 725-731. | 0.9 | 5 |
| 175 | Highly corrosion-resistant amorphous Crî—,Niî—,P alloys. Materials Science & Engineering A: Structural Materials: Properties, Microstructure and Processing, 1994, 181-182, 1114-1118. | 5.6 | 5 |
| 176 | The effect of microcrystallites in the amorphous matrix on the corrosion behavior of amorphous Fe-8Cr-P alloys. Corrosion Science, 1995, 37, 1411-1422. | 6.6 | 5 |
| 177 | The Corrosion Behavior of Ni–Ta–5P Alloys in Concentrated Hydrochloric Acid. Materials Transactions, JIM, 1996, 37, 383-388. | 0.9 | 5 |
| 178 | Hydrogen Evolution Characteristics of Sputter-Deposited Co–Mo, Co–Al and Co–Mo–Al Alloy Electrodes in NaOH Solution. Materials Transactions, JIM, 1998, 39, 1017-1023. | 0.9 | 5 |
| 179 | Hydrogen Embrittlement Behavior of Pure Ni and Ni-20Cr Alloy with Different Grain Sizes. Nippon Kinzoku Gakkaishi/Journal of the Japan Institute of Metals, 2021, 85, 49-58. | 0.4 | 5 |
| 180 | Effects of Static and Dynamic Strain Aging on Hydrogen Embrittlement in TWIP Steels Containing Al. Tetsu-To-Hagane/Journal of the Iron and Steel Institute of Japan, 2014, 100, 1132-1139. | 0.4 | 5 |

| # | Article | IF | CITATIONS |
|-----|--|------|-----------|
| 181 | Hydrogen Entry Behavior into Iron and Steels under Atmospheric Corrosion. Tetsu-To-Hagane/Journal of the Iron and Steel Institute of Japan, 2013, 99, 651-658. | 0.4 | 5 |
| 182 | Realâ€Time Visualization of Hydrogen Distribution in Metals Using Polyaniline: An Ultrasensitive Hydrogenochromic Sensor. Advanced Materials Interfaces, 2022, 9, . | 3.7 | 5 |
| 183 | Hydrogen-accelerated fatigue crack growth of equiatomic Fe–Cr–Ni–Mn–Co high-entropy alloy evaluated by compact tension testing. Materials Science & Engineering A: Structural Materials: Properties, Microstructure and Processing, 2022, 848, 143394. | 5.6 | 5 |
| 184 | Angle-resolved XPS for determination of diffusion coefficients and mobilities of cations in thin passive films. Surface and Interface Analysis, 2000, 30, 106-111. | 1.8 | 4 |
| 185 | Effects of hydrogen content that alters damage evolution mechanisms in SUH 660 precipitation-strengthened Fe–Cr–Ni steel. Materials Science & Engineering A: Structural Materials: Properties, Microstructure and Processing, 2020, 791, 139750. | 5.6 | 4 |
| 186 | Delayed Fracture of High Strength Steels under Atmospheric Corrosion. Zairyo To Kankyo/ Corrosion Engineering, 2011, 60, 184-189. | 0.2 | 4 |
| 187 | Effect of Carbon Content on V-bending in High-Strength TRIP-aided Dual-Phase Steel Sheets with Polygonal Ferrite Matrix. Tetsu-To-Hagane/Journal of the Iron and Steel Institute of Japan, 2020, 106, 934-943. | 0.4 | 4 |
| 188 | Preparation of Protective Alumina Coating on Austenitic Stainless Steel by Sol-Gel Method. Zairyo To Kankyo/ Corrosion Engineering, 1993, 42, 158-165. | 0.2 | 3 |
| 189 | Effect of Strain Rate on the Hydrogen Embrittlement Property of Ultra High-strength Low-alloy TRIP-aided Steel. Tetsu-To-Hagane/Journal of the Iron and Steel Institute of Japan, 2019, 105, 443-451. | 0.4 | 3 |
| 190 | Effect of Carbon Content on V-Bending in High-Strength TRIP-Aided Dual-Phase Steel Sheets with Polygonal Ferrite Matrix. ISIJ International, 2021, 61, 608-616. | 1.4 | 3 |
| 191 | Hydrogen Embrittlement of Metallic Materials and Recent Subjects. Materia Japan, 2017, 56, 230-233. | 0.1 | 3 |
| 192 | Amorphous alloy electrodes for anodic oxidation of sulfite. Materials Science & Engineering A: Structural Materials: Properties, Microstructure and Processing, 1994, 181-182, 1081-1084. | 5.6 | 2 |
| 193 | Effect of phosphorus on the passivation behavior of amorphous Feî—,8Crî—,13Pî—,7C alloy in 9M H2SO4 solution. Materials Science & Engineering A: Structural Materials: Properties, Microstructure and Processing, 1994, 181-182, 1119-1122. | 5.6 | 2 |
| 194 | The Corrosion Behavior of Ni-Cr-Mo Ternary Alloys in Hot Concentrated Sulfuric Acids with Active Carbon (Part 1). Zairyo To Kankyo/ Corrosion Engineering, 1997, 46, 643-650. | 0.2 | 2 |
| 195 | NO decomposition catalysts prepared from amorphous NiTaPd alloys. Applied Catalysis B: Environmental, 1997, 11, 243-255. | 20.2 | 2 |
| 196 | Factors Affecting Static Strain Aging Under Stress at Room Temperature in a Fe-Mn-C Twinning-Induced Plasticity Steel. Tetsu-To-Hagane/Journal of the Iron and Steel Institute of Japan, 2014, 100, 1123-1131. | 0.4 | 2 |
| 197 | Hydrogen Entry into an AISI 4135 High Strength Steel in Tribocorrosion Environment. ECS Transactions, 2017, 75, 33-41. | 0.5 | 2 |
| 198 | Hyperbaric-Oxygen Accelerated Corrosion Test of Iron in Cement Paste and Mortar. Nippon Kinzoku Gakkaishi/Journal of the Japan Institute of Metals, 2018, 82, 1-7. | 0.4 | 2 |

| # | Article | IF | CITATIONS |
|-----|--|-----|-----------|
| 199 | Effects of Matrix Structure and Nitrogen Content on Fatigue Properties of Ultrahigh-Strength Low Alloy TRIP-Aided Steels. ISIJ International, 2021, 61, 591-598. | 1.4 | 2 |
| 200 | Effects of Si and Mn Contents on V-bending in High Strength TRIP-aided Dual-Phase Steel Sheets with Polygonal Ferrite Matrix. Tetsu-To-Hagane/Journal of the Iron and Steel Institute of Japan, 2021, 107, 154-164. | 0.4 | 2 |
| 201 | Effect of Hydrogen on Spot-Welded Tensile Properties in Automotive Ultrahigh-Strength TRIP-Aided Martensitic Steel Sheet. ISIJ International, 2021, 61, 2644-2653. | 1.4 | 2 |
| 202 | XPS Study of Ni-Mo-B Amorphous Ultra-fine Particles Prepared by Chemical Reduction. Nippon Kinzoku Gakkaishi/Journal of the Japan Institute of Metals, 1996, 60, 79-83. | 0.4 | 1 |
| 203 | The sulfidation and oxidation behavior of sputter-deposited Alî—,Nbî—,Mo alloys. Materials Science & Engineering A: Structural Materials: Properties, Microstructure and Processing, 1999, 267, 277-284. | 5.6 | 1 |
| 204 | XPS Determination of Diffusion Coefficients of Cations in Thin Passive Films on Alloys. Solid State Phenomena, 2000, 72, 79-84. | 0.3 | 1 |
| 205 | Acetate and Chloride Effects on Hydrogen Production across Crevices. Materials Science Forum, 2006, 512, 97-102. | 0.3 | 1 |
| 206 | Roles of Hydrogen Content and Pre-strain on Damage Evolution of TRIP-aided Bainitic Ferrite Steel. ISIJ International, 2021, 61, 1309-1314. | 1.4 | 1 |
| 207 | Depressurization-induced diffusionless transformation in pure iron hydrogenated under several gigapascals. Materials Letters: X, 2021, 11, 100078. | 0.7 | 1 |
| 208 | Electrochemical Hydrogen Permeation Tests Under Potentiostatic Hydrogen Charging Conditions Conventionally Used for Hydrogen Embrittlement Study. ECS Meeting Abstracts, 2016, , . | 0.0 | 1 |
| 209 | Effects of Thermomechanical Processing on Hydrogen Embrittlement Properties of UltraHigh-Strength TRIP-Aided Bainitic Ferrite Steels. Metals, 2022, 12, 269. | 2.3 | 1 |
| 210 | Effect of cathodic reduction on catalytic activity of amorphous alloy electrodes for electrooxidation of sulfite. Journal of Applied Electrochemistry, 1995, 25, 953. | 2.9 | 0 |
| 211 | The Microcomposite Structure of Catalysts Prepared by Oxidation of Amorphous Ni–Ta–Pd Alloys. Materials Transactions, JIM, 1997, 38, 123-132. | 0.9 | 0 |
| 212 | Application of Sputter Deposition Technique to the Preparation of Amorphous Alloy-Derived Catalysts for NO Decomposition. Materials Transactions, JIM, 1997, 38, 643-649. | 0.9 | 0 |
| 213 | The Corrosion Behavior of Ni-Cr-Mo Ternary Alloys in Hot Concentrated Sulfuric Acids with Active Carbon (Part 2). Zairyo To Kankyo/ Corrosion Engineering, 1997, 46, 702-708. | 0.2 | 0 |
| 214 | Hydrogen Embrittlement in Al-Added Twinning-Induced Plasticity Steels Evaluated by Tensile Tests during Hydrogen Charging. Tetsu-To-Hagane/Journal of the Iron and Steel Institute of Japan, 2014, 100, 662-667. | 0.4 | 0 |
| 215 | Corrections of the text and the figure in the paper "Effect of Strain Rate on the Hydrogen Embrittlement Property of Ultra High-strength Low Alloy TRIP-aided Steel―[ISIJ International, Vol. 58 (2018), No. 4, pp. 751–759]. ISIJ International, 2018, 58, 1748-1749. | 1.4 | 0 |
| 216 | Effect of Hydrogen on Spot Welded Tensile Properties in Automotive Ultrahigh Strength TRIP-aided Martensitic Steel Sheet. Tetsu-To-Hagane/Journal of the Iron and Steel Institute of Japan, 2021, 107, 175-184. | 0.4 | 0 |

| # | Article | IF | CITATIONS |
|-----|---|------|-----------|
| 217 | Potential Effects of Short-Range Order on Hydrogen Embrittlement of Stable Austenitic Steels—A Review. Advanced Structured Materials, 2021, , 1-18. | 0.5 | 0 |
| 218 | V-bendability of Ultrahigh Strength Low Alloy TRIP-aided Steel Sheets with Bainitic Ferrite Matrix. Tetsu-To-Hagane/Journal of the Iron and Steel Institute of Japan, 2021, 107, 165-174. | 0.4 | 0 |
| 219 | Hydrogen Entry into an AISI 4135 High Strength Steel in Tribocorrosion Environment. ECS Meeting Abstracts, 2016, , . | 0.0 | Ο |
| 220 | Acceleration of Fe Corrosion in Cement Paste and Mortar By Enhancing Oxygen Supply. ECS Meeting Abstracts, 2017, , . | 0.0 | 0 |
| 221 | Electrochemical Hydrogen Permeation Test under Controlled Temperature and Humidity after Outdoor Exposure at Beijing, Chongqing and Okinawa. Tetsu-To-Hagane/Journal of the Iron and Steel Institute of Japan, 2017, 103, 93-100. | 0.4 | Ο |
| 222 | Effect of Interstitial Carbon on Anodic Polarization Behavior of Fe-33Mn-C Austenitic Steels. ECS Meeting Abstracts, 2018, , . | 0.0 | 0 |
| 223 | Size and distribution of micropores and voids in 5052 aluminum alloys during tensile deformation. Keikinzoku/Journal of Japan Institute of Light Metals, 2018, 68, 630-634. | 0.4 | Ο |
| 224 | Corrosion Behavior of Reinforcing Steel with Mill Scale in Concrete. ECS Meeting Abstracts, 2019, , . | 0.0 | 0 |
| 225 | Decomposition of nitrogen monoxide over NiTa2O6-supported palladium catalysts prepared from amorphous alloy precursors. Applied Catalysis B: Environmental, 1996, 9, 93-106. | 20.2 | 0 |